University of California

Real-ESSI Simulator

Multi-Surface Material Model and Tsinghua Liquefaction Model

Yuan Feng
ofeng@ucdavis.edu

supervised by
Prof. Boris Jeremić

30. May, 2017

Contents

Chapter 1

Multi-Surface Plastic Model

Devoted to the expansion and dissemination of knowledge about earthquake, the improvement of earthquake-resistant design, the realistic modeling of soil stress-strain behavior plays a crucial role in the nonlinear finite element analysis. In order to simulate the realistic shear modulus behavior, multi-surface plastic model is proposed by Mroz [5, 4] and further developed by Prevost [6, 7, 8]. Also, Simo and Kennedy [9] developed the integration algorithm for non-smooth multi-surface material model. In Real-ESSI simulator, multi-surface material model is employed to match the G/Gmax curves by piecewise linear curves.

As the name implies, multi-surface model is composed of multiple yield surface in the deviatoric stress space. For each yield surface, the stress-strain curve is linear. The shear modulus becomes smaller after the stress states exceed each yield surface.

1.1 Multi-Surface Material Model

As shown in Fig. 1.1, the multi-surface material model applies the multiple yield surface to control the shear modulus reduction precisely.

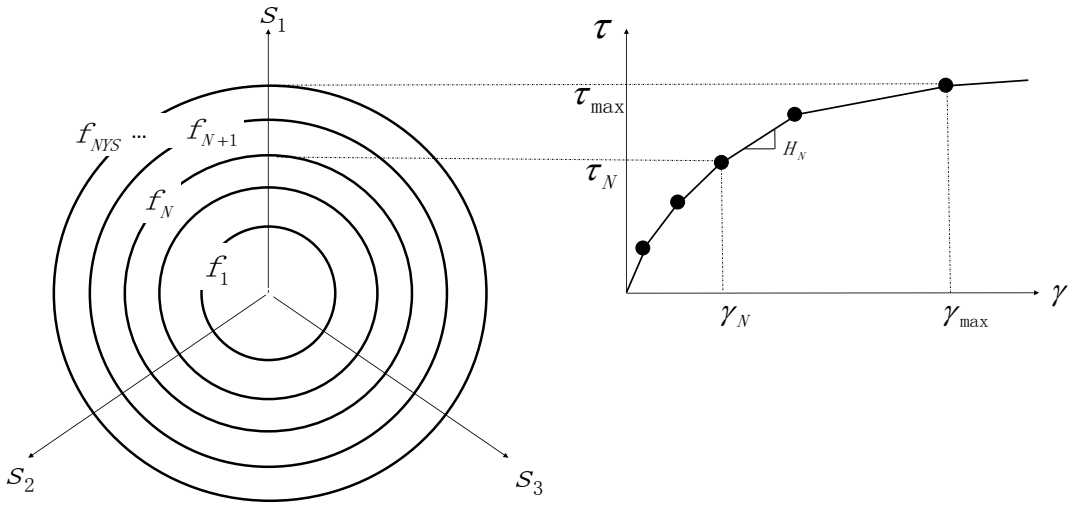

Figure 1.1: Multi-surface Material Model with G/Gmax

Elasticity The constitutive equations are written in

$$d\sigma_{ij} = E_{ijkl}(d\epsilon_{kl} - d\epsilon_{kl}^{plastic}) \tag{1.1}$$

where $d\sigma_{ij}$ is the effective stress increment, $d\epsilon_{kl}$ is the total strain increment, and $d\epsilon_{kl}^{plastic}$ is the plastic strain increment. And E_{ijkl} is the isotropic elastic coefficient tensor.

$$E_{ijkl} = (B - 2G/3)\delta_{ij}\delta_{kl} + G(\delta_{ik}\delta_{jl} + \delta_{il}\delta_{jk}) \tag{1.2}$$

where B is the bulk modulus and G is the shear modulus.

The dependence of the modulus upon the effective mean stress is

$$G = G_0(\frac{p}{p_0})^n \qquad B = B_0(\frac{p}{p_0})^n \qquad H = H_0(\frac{p}{p_0})^n \tag{1.3}$$

where n is the experimental parameter. And p_0 is the reference pressure.

Yield Function Three yield surfaces are implementated for multi-surface plasticity, including von-Mises material, Drucker-Prager material, and rounded Mohr-Coulumb yield surface. The Rounded Mohr-Coulumb yield condition is

$$\bar{f} = \frac{3}{2}(s_{ij} - p\alpha_{ij})(s_{ij} - p\alpha_{ij}) - R^2(\theta)r^2p^2 = 0 \tag{1.4}$$

where

$$R(\theta) = \frac{2k}{(1+k) - (1-k)sin3\theta} \tag{1.5}$$

where k is a material constant which controls the shape of the cross section of the yield surface. When $k = 1$, the cross section is a circle, which is equivalent to the Drucker-Prager yield surface. And, θ is the Lode angle written in

$$\begin{aligned} sin3\theta &= -\sqrt{6}\bar{J}_3/(\bar{J}_2)^{3/2} \\ \bar{J}_2 &= s_{ij}s_{ij} \\ \bar{J}_3 &= 3\ det(\bar{s}_{ij}) \end{aligned} \tag{1.6}$$

with

$$\bar{s}_{ij} = 3(s_{ij} - p\alpha_{ij}) \tag{1.7}$$

Note that the deviatoric stress invariants defined here are different from the conventional deviatoric stress invariants on purpose.

Note that in the yield surface function in Eq. 1.4 ,

- When the material parameter k is 1, the yield surface is equivalent to Drucker-Prager.
- When the influence of pressure p is removed, the yield surface is equivalent to von-Mises.

Plastic Flow Rule The plastic flow rule is controlled by the stress-ratio. The deviatoric plastic flow is associative, while the volumetric component is non-associative.

$$\begin{aligned} m^{dev} &= n^{dev} \\ m^{vol} &= \frac{1}{3}\frac{(\eta/\bar{\eta})^2 - 1}{(\eta/\bar{\eta})^2 + 1} \end{aligned} \tag{1.8}$$

where $\eta = (\frac{3}{2}s_{ij}s_{ij})^{1/2}/p$ is the stress ratio. And $\bar{\eta}$ is the material parameter.

- When $\eta < \bar{\eta}$, the material takes plastic compaction.
- When $\eta > \bar{\eta}$, the material takes plastic dilation.
- When $\eta = \bar{\eta}$, the material takes no volumetric change.

Hardening Rule In the framework of classical elastoplastic material model, multi-surface is nothing but a sophisticated hardening rule.

The direction of the hardening rule is selected to avoid the overlappings of surfaces (which would lead to a non-unique definition of the constitutive theory), so the direction of translation μ of the active yield surface is

$$\mu_{ij} = \frac{r'}{r}(s_{ij} - p\alpha_{ij}) - (s_{ij} - p\alpha'_{ij}) \tag{1.9}$$

where r and α_{ij} is the size and center of the current active yield surface. r' and α'_{ij} is the size and center of the next larger yield surface. And $r' > r$.

1.2 Multi-Surface Material Model Integration Algorithms

In the single yield-surface integration algorithm, the return mapping algorithm is a two-step algorithm. The first step is the elastic prediction. The second step is the plastic correction. The plastic correction returns the stress state onto the single yield surface.

In the multi-surface integration algorithm, the plastic corrector returns onto the current active yield surface but may be outside the next larger yield surface. In this case, the plastic correction should be calculated again with respect to the next larger yield surface. However, one crucial correction must be made to take account of the fact that the stress has been over-relaxed. Therefore, the stress should be corrected back to a new trial stress with respect to the ratio of the different plastic modulus between two yield surfaces. Then, the stress state is corrected back to the next larger yield surface from the new trial stress state.

Compared to the single yield surface algorithm, multi-surface algorithm has one more unknown, namely, the center (backstress) of the next larger yield surface. Meantime, multi-surface algorithm has one more equation, namely, the contact condition between the two yield surface functions, as shown in Fig. 1.2. Therefore, we can still solve the multi-surface plasticity equations. In addition, after the converge of the second yield surface, remember to check the next larger yield-surface again and to resume the over-relax correction if necessary until all the yield surface are active. After the stress update, the inner yield surfaces are updated again to maintain the contact condition between yield-surfaces.

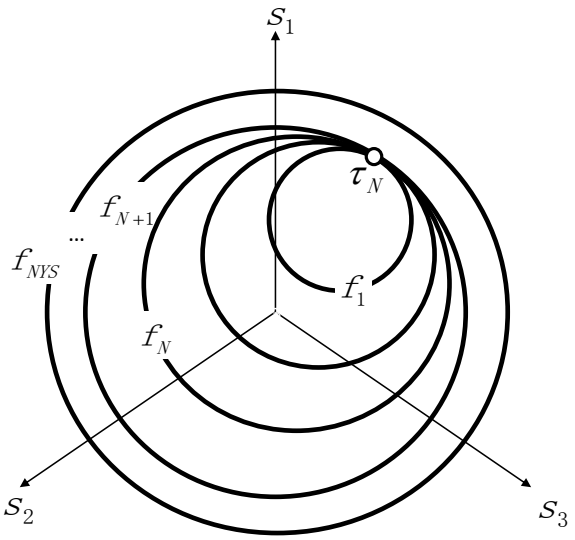

Figure 1.2: Contact Condition in Multi-surface Material Model

So the plastic strain calculation process thus becomes

$$\epsilon_{ij}^{pl(I+1)} = \epsilon_{ij}^{pl(I)} - \lambda_N^I m_{ij(N)}(\sigma^I, \alpha_N^I) + \lambda_{N+1}^I m_{ij(N+1)}(\sigma^I, \alpha_{N+1}^I) \tag{1.10}$$

$$\alpha_{ij(N)}^{pl(I+1)} = \alpha_{ij(N)}^{pl(I)} - \lambda_N^I \bar{\alpha}_{ij(N)}(\sigma^I, \alpha_N^I) \tag{1.11}$$

$$\alpha_{ij(N+1)}^{pl(I+1)} = \alpha_{ij(N+1)}^{pl(I)} + \lambda_{N+1}^I \bar{\alpha}_{ij(N+1)}(\sigma^I, \alpha_{N+1}^I) \tag{1.12}$$

$$\sigma_{ij}^{pl(I+1)} = \sigma_{ij}^{pl(I)} + \lambda_N^I E_{ijkl} \bar{\alpha}_{kl(N)}(\sigma^I, \alpha_N^I) - \lambda_{N+1}^I E_{ijkl} \bar{\alpha}_{kl(N+1)}(\sigma^I, \alpha_{N+1}^I) \tag{1.13}$$

where the superscript I represents the iteration number, the subscript N represents the number of active yield surface, the tensor $\bar{\alpha}$ represents the rate (hardening rule) of the backstress α. The length λ_N is determined by linearizing the yield function $f_{(N)}$ about the current values of the state variables

$$f_N(\sigma^I, \alpha_N^{I+1}) = f_N(\sigma^I, \alpha_N^I) + \frac{\partial f_N}{\partial \alpha_{ij}}(\alpha_{ij(N)}^{I+1} - \alpha_{ij(N)}^I) \tag{1.14}$$

and the new condition of yield surface contact.

$$f_N(\sigma^I, \alpha_N^{I+1}) = f_{N+1}(\sigma^I, \alpha_{N+1}^I) \tag{1.15}$$

Then, since $f_N(\sigma^I, \alpha_N^I) = 0$, and combine Eq 1.11, 1.14, 1.15, resulting the plastic multiplier λ_N for current yield surface

$$\lambda_N^I = -\frac{f_{N+1}(\sigma^I, \alpha_{N+1}^I)}{\partial_\alpha f_N : \bar{\alpha}_N(\sigma^I, \alpha_N^I)} = \frac{f_{N+1}(\sigma^I, \alpha_{N+1}^I)}{H_N'^I} \tag{1.16}$$

where H' is the plastic hardening components expressed as

$$H'_N = -\frac{\partial f}{\partial \alpha_N} : \bar{\alpha}_N \tag{1.17}$$

The plastic multiplier λ_{N+1} for the next yield surface is determined by linearizing the yield function f_{N+1} with respect to current backstress α_N

$$\begin{aligned} f_{N+1}(\sigma^{I+1}, \alpha^{I+1}_{N+1}) \approx & f_{N+1}(\sigma^I, \alpha^I_{N+1}) \\ & + \partial_\sigma f_{N+1} : (\sigma^{I+1} - \sigma^I) + \partial_\alpha f_{N+1} : (\alpha^{I+1}_{N+1} - \alpha^I_{N+1}) \end{aligned} \tag{1.18}$$

Combine Eq 1.10, 1.11, 1.12, 1.13, 1.16, and 1.18, resulting

$$\lambda^I_{N+1} = \frac{f_{N+1}(\sigma^I, \alpha^I_{N+1})}{n_{N+1} : E : m_{N+1} - \partial_\alpha f_{N+1} : \bar{\alpha}_{N+1}} \left(1 + \frac{n_{N+1} : E : m_N}{H'^I_N}\right). \tag{1.19}$$

where n is the normal to the yield surface, where m is the plastic flow rule defined in Eq. 1.8,

The procedures are summarized in the Flowchart 1.

Algorithm 1 Integration algorithm for multi-surface plasticity

procedure MULTI-SURFACE PLASTICITY INTEGRATION($d\epsilon$) ▷ Input Strain Increment
  Step 1. Initialize: I=0, N=1, $\epsilon^{pl} = \epsilon^{pl}, \alpha_{(N)} = 0$.
  Step 2. Update stress and check yield condition / plastic consistency:
    $\sigma = E : (\epsilon - \epsilon^{pl})$.
    $f_N = f_N(\sigma, \alpha_N)$.
    IF $\|f_N \leq 0\|$
      Go to Step 6.
    End IF
  Step 3. Compute new plastic loading function:
    $\bar{\lambda} = \left[\frac{f_N}{n_N : E : m_N - \frac{\partial f}{\partial \alpha_N} : \bar{\alpha}_N}\right]$.
  Step 4. Update plastic strains and state variables:
    $\epsilon^{pl(I+1)} = \epsilon^{pl(I)} + \bar{\lambda} m_N$
    $\alpha^{pl(I+1)} = \alpha^{pl(I)} + \bar{\lambda} \bar{\alpha}_N$
  Step 5. Next iteration: I = I + 1 and Go to Step 2.
  Step 6. Check for overshooting of next yield surface, f^{N+1} :
    IF N = NYS EXIT ▷ NYS is the total number of yield surface.
    IF $f_{N+1}(\sigma, \alpha_{N+1}) \leq 0$ EXIT
    ELSE Go to Step 7.
  Step 7. Compute new plastic loading functions:
    $H_N = n_N : E : m_N$ $H'_N = -\frac{f}{\alpha_N} : E : \bar{\alpha}_N$
    $\lambda_N = \frac{f_{N+1}}{H'_N}$ $\lambda_{N+1} = \left[\frac{f_{N+1}}{H_{N+1} + H'_{N+1}}(1 + \frac{H_N}{H'_N})\right]$.
  Step 8. Update plastic strains and state variables:
    $\epsilon^{pl(I+1)}_{N+1} = \epsilon^{pl(I)}_{N+1} - \lambda_N m_N + \lambda_{N+1} m_{N+1}$.
    $\alpha^{I+1}_{N+1} = \alpha^I_{N+1} + \lambda_{N+1} \bar{\alpha}_{N+1}$.
  Step 9. Next yield surface: N = N + 1 ; I = I + 1; and Go to Step 2.
end procedure

1.3 Multi-Surface Material Model Realistic Behavior on G/Gmax

Below are the G/Gmax and damping plot for Multi-Yield-Surface von-Mises.

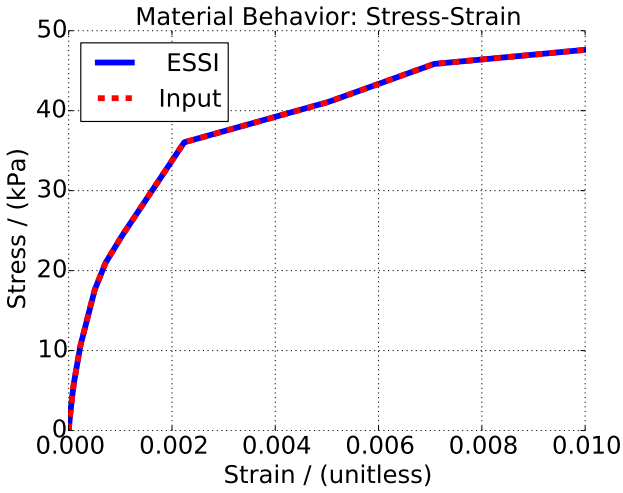

(a) Stress-Strain Curves

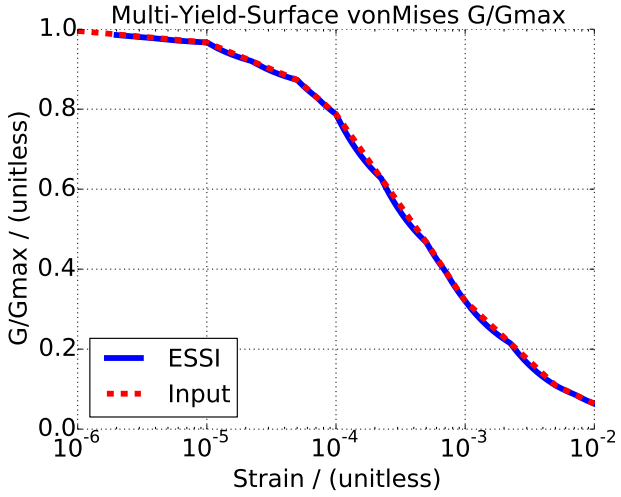

(b) G/Gmax Comparison

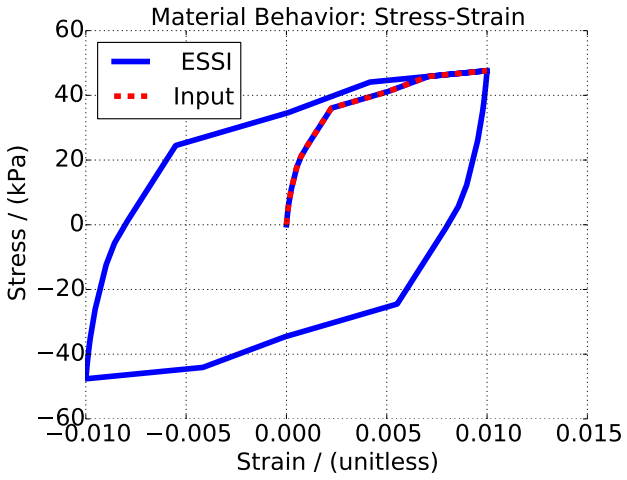

(c) One Cyclic Stress-Strain Curves

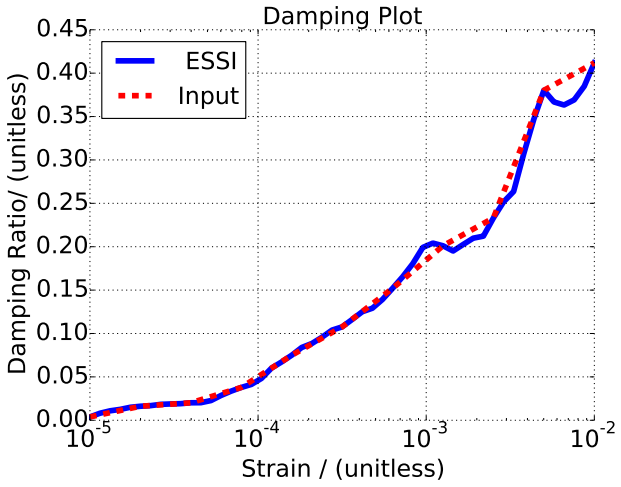

(d) Damping Plot Curves

Figure 1.3: Multi-Yield-Surface von-Mises

1.4 Multi-Surface Material Model Realistic Behavior under Cyclic Loading

Figure 1.4 shows the model prediction of a cyclic pure shear test simulation. In the test, the shear stress amplitude $30kPa$ is kept constant. The hysteretic response of the material is shown in Figure 1.4, the material softens and the shear strain amplitude increases as a result of cycling.

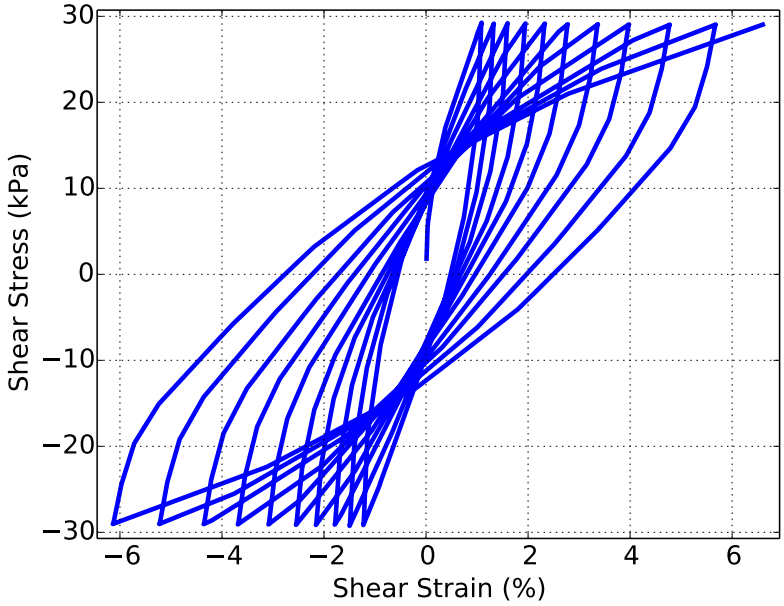

Figure 1.4: Shear Behavior under Cyclic Loading

Chapter 2

Bounding-Surface Plasticity

2.1 Bounding-Surface Material Model – Tsinghua Liquefaction

Bounding-surface plastic model was developed by Dafalias [1, 3, 2]. In addition to the existing yield surface, another larger surface was proposed to limit the material strength.

Tsinghua Liquefaction material model is built on top of the bounding-surface model. The purpose of Tsinghua Liquefaction constitutive material model is to simulate the large-deformation after the liquefaction. According to the experimental data, the pore pressure after the initial liquefaction has two parts, including the reversible and irreversible pore pressure. Based on this phenomenon, Gang Wang and Jianmin Zhang ([10, 11]) developed the Tsinghua Liquefaction constitutive model on the top of the bounding-surface model. The volumetric plastic strain is divided into reversible and irreversible strain to echo the experimental results. The general formulation of the Tsinghua Liquefaction material model is as follows.

In the absence of rate-dependent behavior, the strain rates can equivalently be used instead of strain increments.

$$\dot{\varepsilon} = \dot{\varepsilon}^e + \dot{\varepsilon}^p \tag{2.1}$$

where $\dot{\varepsilon}, \dot{\varepsilon}^e, \dot{\varepsilon}^p$ denote the strain rate tensor and its elastic and plastic parts, respectively. The elastic strain can be determined by a generalized Hooke's law,

$$\dot{\varepsilon}^e = \dot{e}^e + \frac{1}{3}\dot{\varepsilon}_v I = \frac{1}{2G}\dot{s} + \frac{1}{3K}\dot{p}I \tag{2.2}$$

in which G and K are, respectively, elastic shear and bulk modulus. Their dependence both on material state and on effective stress state.

The plastic response can be induced due to two different and superposed mechanisms. The first mechanism is associated with the shear stress ratio r, known as shear yielding mechanism, and the second, with change in mean effective stress p, known as compression mechanism. In the present model, only the first mechanism is taken into consideration for simplicity. To this end, the following plastic loading intensity L can be defined.

$$L = p\dot{r} : n \tag{2.3}$$

in which n is the loading direction in stress ratio space. Loading or unloading is defined by the sign of L, i.e., positive for loading and negative for unloading. In case of loading, plastic deformation will be generated. The plastic hardening criterion is assumed as

$$\dot{\lambda} = \dot{\gamma}^p = \frac{\langle L \rangle}{H} = \frac{\langle p\ \dot{r} : n \rangle}{H} \tag{2.4}$$

where λ is the plastic multiplier, and H is the plastic modulus. $\langle\rangle$ is the Macauley brackets. The rate of the plastic deviatoric strain can be written as

$$\dot{e}^p = m\dot{\gamma}^p = m\frac{\langle p\ \dot{r} : n\rangle}{H} \tag{2.5}$$

in which m is a zero trace tensor defining the direction of plastic deviatoric strain increment.

The volumetric strain induced due to shear is composed of an irreversible component and a reversible component. But according to current laws of elasticity, elastic shearing does not cause volumetric change. Therefore, both dilatancy components are assumed as plastic ones in the present model. They can be written as

$$\dot{\varepsilon}_{vd,re} = \dot{\varepsilon}^p_{vd,re} = D_{re}\dot{\gamma}^p = D_{re}\frac{\langle p\ \dot{r} : n\rangle}{H} \tag{2.6}$$

$$\dot{\varepsilon}_{vd,ir} = \dot{\varepsilon}^p_{vd,ir} = D_{ir}\dot{\gamma}^p = D_{ir}\frac{\langle p\ \dot{r} : n\rangle}{H} \tag{2.7}$$

where D_{re} and D_{ir} are the reversible and irreversible dilatancy rates, respectively.

The total strain rate can be obtained by adding Eq 2.2, 2.5, 2.6, 2.7 together.

$$\varepsilon = \frac{1}{2G}p\dot{r} + (\frac{r}{2G} + \frac{I}{3K})\dot{p} + (m + \frac{D_{re} + D_{ir}}{3}I)\frac{\langle p\ \dot{r} : n\rangle}{H} \tag{2.8}$$

The above constitutive equation has the following ingredients: (a) elastic shear and bulk moduli G and K; (b) loading and flow direction n and m in the stress ratio space; (c) plastic modulus H; and (d) dilatancy function D_{re} and D_{ir} . These quantities will be specified in the following section.

This is the general formulation for the Tsinghua Liquefaction material model. The author translated the Fortran imperative programming to C++ object-oriented programming. The author will then accelerate the C++ implementation with all kinds of small linear algebra technique. For the detailed information about the constitutive model, please refer to the original paper [11, 10].

2.1.1 Reversible dilatancy parameters

The key part in Tsinghua material model is the separation between the reversible and irreversible dilatancy material behavior. The parameters $M_{d,c}$ and d_{re1} among the three reversible dilatancy parameters are important for the reversible dilatancy rate. Note that $M_{d,c}$ is not the phase transformation shear stress ratio, because we decompose the total dilatancy into two parts. The irreversible dilatancy has a significant impact on the stress-dilatancy behavior only in the range immediately after the stress reversal. Along with further increasing shear strain, however, the irreversible dilatancy diminishes and the reversible dilatancy becomes dominant.

2.1.2 Irreversible dilatancy parameters

Determining the three irreversible dilatancy parameters α, d_{ir}, and $\gamma_{d,r}$ are the most important parts. These three parameters control both the pore pressure in the pre-liquefaction regime and the shear strain in the post-liquefaction regime. Because of its strong dependence on both the initial density and confining pressure, the irreversible dilatancy rate under undrained condition is considerably different from that under drained condition. Therefore, the three parameters cannot be determined by a single drained cyclic test.

2.2 Material Performance

The cyclic stress-controlled triaxial tests was simulated. In the simulation, all the specimens were assumed isotropically consolidated to a confining stress of 100 kPa. The initial back stress ratio was zero, and the initial bounding surface ratio $\eta_m = 0$. Strain increment controlled calculation was employed. First, the cyclic axial strain increment $\triangle\epsilon_z$ was applied, in the meanwhile, let two lateral strain increment $\triangle\epsilon_x$=$\triangle\epsilon_y$=0.5$\triangle\epsilon_z$ to ensure undrained conditions. When the axial stress reached the cyclic stress amplitude, the axial strain increment was reversed. The maximum strength ratio of triaxial compression to triaxial extension was assume to be 0.65. Fig. 2.1 and Fig. 2.2 give a comparison of the liquefaction strength curves obtained from the model simulation against the test results. Simulation gives a relative good simulation for both loose sand ($e_0 = 0.585$) and dense sand ($e_0 = 0.515$). The loose sand goes to liquefaction faster than the dense sand.

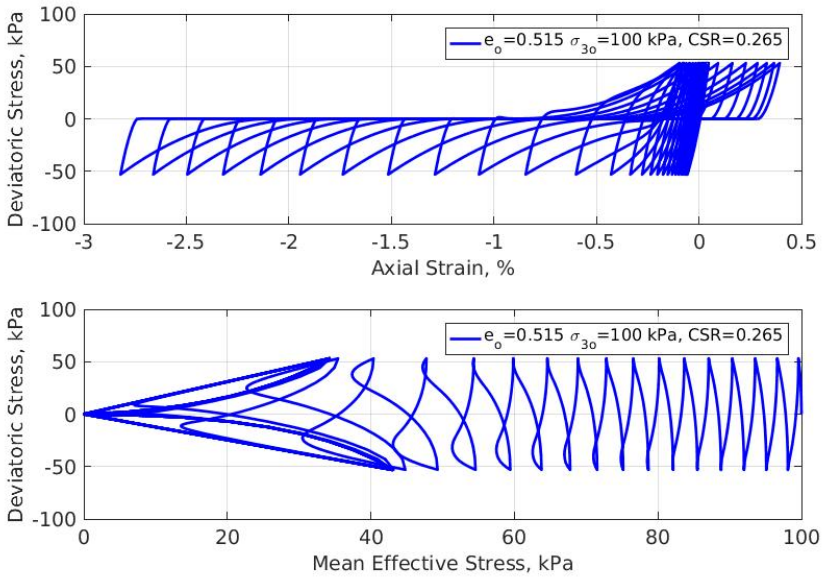

Figure 2.1: Material Behavior of Tsinghua Material Model

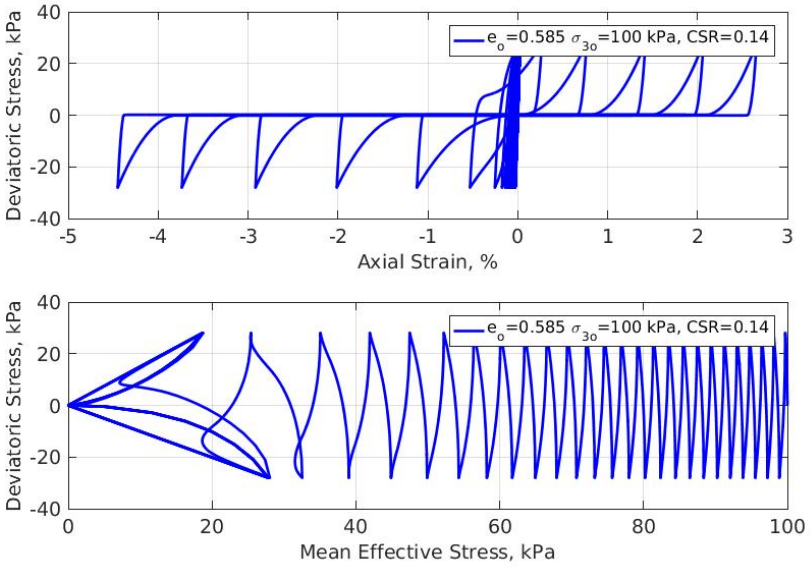

Figure 2.2: Material Behavior of Tsinghua Material Model

Chapter 3

Comparison between Bounding Surface and Multi-Surface

3.1 Multi-surfaces plasticity

In the theory of multi-surface plasticity, a series of plastic modulus is used to represent the shear modulus reduction during the earthquake. The stress field is dividid by the nested yield surfaces f_1, f_2, ..., f_b with the respective sizes $k^{(1)} < k^{(2)} < ... < k^{(b)}$. The divided fields are associated with the corresponding shear modulus. Inside the first (smallest) yield surface, the material behaviour is purely elastic. The outermost yield surface, f_b plays the role of a failure (bounding) surface. When the stress exceeds one yield surface, the stress is corrected back and the corresponding yield surfaces become the active yield surfaces. All active yield surfaces may be translated in the stress space with the consecutively touching. The active yield surfaces contact each other without overlapping. Whenever one yield surface is activated, the shear modulus is decreased to the corresponding shear modulus. Unloading deactives the yield surfaces if the stress becomes inside the yield surfaces, which is similar to the single yield-surface plasticity. Multi-Surface model can be accurately calibrated with the experimental shear modulus. But multi-Surface model requires excessive memory usage to store all the back-stress of each yield surface.

3.2 Two-surfaces plasticity

In the two-surfaces plasticity, only the first and the last yield surfaces (f_1 and f_b) are retained. The intermediate surfaces are replaced by an analytical function. Then, the first yield surface f_1 is called the loading surface, and the last yield surface f_b is called the bounding surface. The hardening rule is prescribed by the two surfaces. Two distances are employed to define the modulus. One is the distance between back-stress and yield-stress of the loading surface. The other one is the distance between back-stress and the projection of yield-stress on the bounding surface. The ratio between the projection-distance and original distance controls the hardening modulus. When the stress approaches the bounding surface, the ratio of the distance decreases such that the rate of the stress change is approaching zero. In this way, the bounding surface works like the final boundary of the stress states.

In addition, the back-stress of the loading surface is also called the reversal point. In Tsinghua liquefaction bounding surface model, the reversal point is fixed during the loading process. When it starts unloading, the old reversal point is replaced by the current stress state at the intersection point between the loading and unloading. When the direction angle between two loading steps is smaller than 90°, the next loading step is taken as the loading process. Otherwise, the next loading step is taken as the unloading process.

As we can see, during the computation process of hardening modulus, only the reversal point is required for storage. The intermediate hardening modulus is estimated by the analytical function, which might be interpolated from the experiments. This method saves memory for each material point, compared to the multi-surface plasticity. In the realistic large-scale numerical model, millions of material points are required during the simulation. The saved memory at one material point can save much more memory in the global level. However, this analytical function of the hardening modulus becomes more complicated to be calibrated with the physical experiments.

Bibliography

[1] Yannis F. Dafalias. Bounding surface plasticity. I: Mathematical foundations and hypoplasticity. *ASCE Journal of Engineering Mechanics*, 112(9):966–987, September 1986.

[2] Yannis F. Dafalias and Majid T. Manzari. Simple plasticity sand model accounting for fabric change effects. *ASCE Journal of Engineering Mechanics*, 130(6):622–634, June 2004.

[3] M. T. Manzari and Y. F. Dafalias. A critical state two–surface plasticity model for sands. *Géotechnique*, 47(2):255–272, 1997.

[4] Z. Mroz and V. A. Norris. Elastoplastic and viscoplastic constitutive models for soils with application to cyclic loadings. In G. N. Pande and O. C. Zienkiewicz, editors, *Soil Mechanics – Transient and Cyclic Loads*, pages 173–217. John Wiley and Sons Ltd., 1982.

[5] Z. Mróz, V. A. Norris, and O. C. Zienkiewicz. Application of an anisotropic hardening model in the analysis of elasto–plastic deformation of soils. *Géotechnique*, 29(1):1–34, 1979.

[6] Jean H. Prevost. A simple plasticity theory for frictional cohesionless soils. *International Journal of Soil Dynamics and Earthquake Engineering*, 4(1):9 – 17, 1985.

[7] Jean H Prevost. *DYNA1D: a computer program for nonlinear seismic site response analysis technical documentation*. National Center for Earthquake Engineering Research, 1989.

[8] Jean H. Prevost and Radu Popescu. Constitutive relations for soil materials. *Electronic Journal of Geotechnical Engineering*, October 1996. available at http://139.78.66.61/ejge/.

[9] J. C. Simo, J. G. Kennedy, and S. Govindjee. Non - smooth multisurface plasticity and viscoplasticity. loading / unloading, conditions and numerical algorithms. *International Journal for Numerical Methods in Engineering*, 26:2161–2185, 1988.

[10] Rui Wang, Jian-Min Zhang, and Gang Wang. A unified plasticity model for large post-liquefaction shear deformation of sand. *Computers and Geotechnics*, 59:54–66, 2014.

[11] Jian-Min Zhang and Gang Wang. Large post-liquefaction deformation of sand, part i: physical mechanism, constitutive description and numerical algorithm. *Acta Geotechnica*, 7(2):69–113, 2012.